TABLE III (*Footnotes*)

[a] The number in parentheses is the standard deviation in the least significant digit as calculated from the standard deviations of coordinates. [b] The standard deviations of 0.015 Å and 1° listed for average values are based upon comparisons of distances expected to be the same and the authors' past experience. They are believed to be better representations of the accuracy of these results than those calculated from the standard deviations of coordinates. [c] The two corrections for thermal motion given are a minimum correction and a "riding-model" correction, respectively. Both are much less than the maximum possible correction. (See text and ref 10.) [d] "Tables of Interatomic Distances and Configuration in Molecules and Ions," Special Publication No. 11, The Chemical Society, Burlington House, London, 1958, p M18. [e] L. Trefonas and W. N. Lipscomb, *J. Chem. Phys.*, **28**, 54 (1958). [f] R. L. Kuczkowski and D. R. Lide, Jr., *ibid.*, **46**, 357 (1967) (microwave study). [g] Q. Williams, J. Sheridan, and W. Gordy, *ibid.*, **20**, 164 (1952) (microwave and electron diffraction study). [h] Numbers in brackets are the authors' calculation from cell dimensions and positional parameters given (X-ray crystallographic study).

propeller-like configuration. The observation that each fluorine has at least two intermolecular F–F contacts shorter than any intramolecular one (except between two fluorines bonded to the same atom) shows that the fluorine contacts within the molecule are not short enough to control the configuration. The BF_2 orientations are evidently governed by the meshing together of fluorine atoms on adjacent molecules (see Figure 2). The existence of intermolecular F–F contacts shorter than the intramolecular ones also indicates that the B–P distance is not controlled by F–F interactions. This, and the fact that the B–P distance found here is not significantly different from that found for $H_3B \cdot PF_3$, indicates that BF_2 will not only formally replace hydrogen[3] but is also quite similar to hydrogen in its electronic effects on the rest of the molecule.

Inspection of the magnitudes and directions of the principal axes of the thermal ellipsoids reveals that the greatest anisotropy is in the motion of the fluorine atoms and that the largest amplitudes are in directions which are more or less perpendicular to bond directions. A considerable component of this motion may consist of librations of the PF_3 and BF_2 groups about the directions of their bonds to the central boron atom, but bending vibrations also appear to be important.

Acknowledgment.—We thank Professor Timms for providing the samples which made this work possible and for providing them in such a convenient form. We also thank Professor Timms and Mr. Ralph Kirk for helpful discussions regarding the significance of these results.

CONTRIBUTION NO. 1463 FROM THE CENTRAL RESEARCH DEPARTMENT,
E. I. DU PONT DE NEMOURS AND COMPANY, EXPERIMENTAL STATION, WILMINGTON, DELAWARE 19898

Crystal Chemistry of Metal Dioxides with Rutile-Related Structures

BY D. B. ROGERS, R. D. SHANNON, A. W. SLEIGHT, AND J. L. GILLSON

Received May 20, 1968

In order to attempt a systematic correlation of the crystal chemistries of the transition metal dioxides with rutile-related structures, single crystals were grown of the oxides MO_2, where M = Mn, Mo, Ru, W, Re, Os, or Ir, and certain electrical transport and crystallographic parameters were accurately determined. Trends of these parameters within the rutile family are shown to be closely associated with variations in the occupancy of the transition metal d shells. Qualitative, one-electron energy level diagrams are discussed that appear to rationalize the electrical and crystallographic properties of these materials.

Introduction

Many metal dioxides, particularly those of the transition metals, crystallize in structural types that are closely related to that of the rutile form of TiO_2 (Figure 1). The properties of rutile were extensively discussed by Grant,[1] and structural reviews of most of the related dioxides and of compounds possessing the similar trirutile structure have been given by Baur[2] and Bayer.[3] The dioxides of Cr, Os, Ru, Ir, Sn, and Ta are tetragonal and isomorphous with rutile; those of V, Nb, Mo, Tc, and W adopt distorted variants of the rutile structure in which the metal atoms occur in pairs along the *c* axis of the rutile pseudocell. Most of the latter oxides are monoclinic and are characterized by a tilt of the metal atom doublets in the [100] direction of the rutile subcell. NbO_2, however, is tetragonal and

(1) F. A. Grant, *Rev. Mod. Phys.*, **31**, 646 (1959).

(2) W. H. Baur, *Acta Cryst.*, **9**, 515 (1956).

(3) G. Bayer, *Ber. Deut. Keram. Ges.*, **39**, 535 (1962).

the doublets are tilted along either the [110] or [1$\bar{1}$0] direction.[4] SiO_2, GeO_2, TiO_2, MnO_2, and PbO_2 are polymorphous with one modification that is isostructural with tetragonal rutile. ReO_2 is also polymorphous, and when synthesized below about 300°, the structural modification (α) is that of monoclinic MoO_2. Above about 300° this oxide transforms irreversibly to an orthorhombic from (β) with a structure characterized by zigzag chains of Re atoms propagating along the c axis of the unit cell.[5,6] A similar modification is found for α-PbO_2. Recently, rutile-type structures have been reported for RhO_2 and for PtO_2.[7] The platinum compound has orthorhombic symmetry.

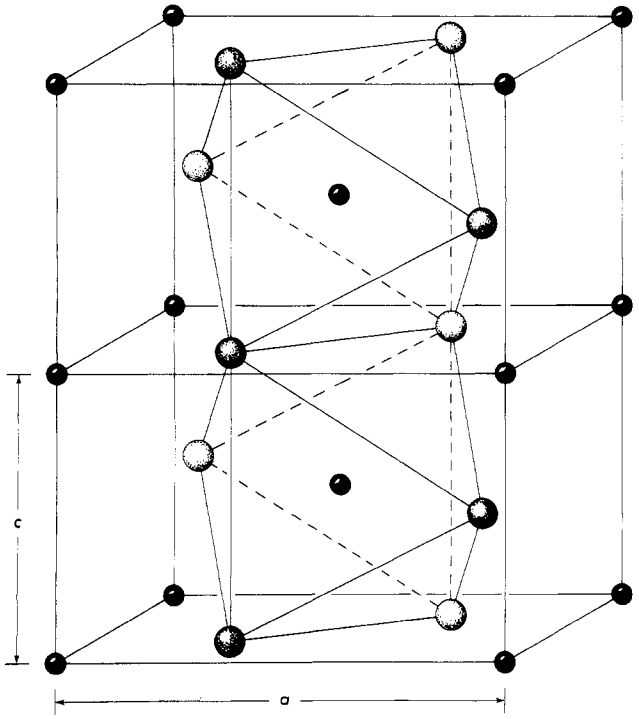

Figure 1.—The structure of rutile.

The transition metals that form dioxides with rutile-related structures have incompletely filled d shells. Variation in the occupancy of these shells accounts for the variety of properties that are observed for these materials and, presumably, for their modifications in structure. Both Magnéli and coworkers[8-11] and Goodenough[12,13] have pointed out certain trends within the rutile family as functions of d-electron number. In particular, Goodenough proposed a qualitative model that appeared to rationalize many of the properties of TiO_2, VO_2, MoO_2, and WO_2. However, since many members of this family have been inadequately characterized, more extensive correlations have been difficult. Several questions have been raised in the literature, particularly about the dioxides of the platinum group metals. Schäfer, *et al.*,[14] have remarked about the low room-temperature resistivity (~50μ ohm-cm) of RuO_2, and Cotton and Mague[15] have noted that the magnetic susceptibility of this oxide is very low in spite of the fact that the Ru–Ru distance is too great for significant direct metal–metal interactions. Recently, Fletcher, *et al.*,[16] have confirmed metal-like conductivity for RuO_2 and proposed that this property implies "that the average oxidation state of the ruthenium atoms is substantially greater than +4."

It seemed to us in view of the apparent success of Goodenough's model as applied to some of the rutile-related dioxides that a suitably modified version would have general applicability to the entire series. In order to determine such applicability, we have attempted to obtain electrical conductivity data and accurate cell dimensions for those members of the series where such data were lacking. Single crystals were desirable for the electrical measurements, and therefore MnO_2, MoO_2, RuO_2, WO_2, β-ReO_2, OsO_2, and IrO_2 were synthesized in single-crystal form. For two of these, MnO_2 and β-ReO_2, crystal growth has not been described previously; for two others, MoO_2 and WO_2, novel growth techniques are reported. The data obtained in our study, combined with reliable data previously reported, now permit an extensive correlation of the structural features and electrical transport behavior of the rutile family of transition metal dioxides. Modifications of Goodenough's original model are proposed that seem to rationalize most of the observed properties.

Experimental Section

The dioxides of Mn, Mo, Ru, Rh, W, Re, Os, Ir, and Pt were prepared in this investigation. Single crystals of RuO_2, IrO_2, and OsO_2 were grown by direct oxidation of their respective metals in the presence of excess oxygen using modifications of the general procedures described by Schäfer.[17] These procedures take advantage of chemical transport from a hotter temperature (T_2) to a cooler temperature (T_1) *via* volatile higher oxides. Ruthenium and iridium dioxides were grown in a stream of oxygen using metals of high purity (greater than 99.99%) and reaction temperatures (T_2) of 1000 and 1050°, respectively. In both cases deposition of the dioxides as single crystals occurred downstream at lower temperatures. RuO_2 crystals were tabular and 1–2 mm in length, whereas IrO_2 crystals generally possessed a needle-like habit and were somewhat smaller. Golden equidimensional crystals of OsO_2 with well-developed faces were grown by the oxidation of high-purity osmium with excess $NaClO_3$

(4) B.-O. Marinder, *Arkiv Kemi*, **19**, 435 (1962).
(5) A. Magnéli, *Acta Cryst.*, **9**, 1038 (1956).
(6) A. Magnéli, *Acta Chem. Scand.*, **11**, 28 (1957).
(7) R. D. Shannon, *Solid State Commun.*, **6**, 139 (1968).
(8) A. Magnéli and G. Anderson, *Acta Chem. Scand.*, **9**, 1378 (1955).
(9) B.-O. Marinder and A. Magnéli, *ibid.*, **12**, 1345 (1958).
(10) B.-O. Marinder and A. Magnéli, *ibid.*, **11**, 1635 (1957).
(11) B.-O. Marinder, E. Dorm, and M. Seleborg, *ibid.*, **16**, 293 (1962).
(12) J. B. Goodenough, "Magnetism and the Chemical Bond," Interscience Monographs on Chemistry, Inorganic Chemistry Section, Vol. 1, F. A. Cotton, Ed., Interscience Division, John Wiley & Sons, Inc., New York, N. Y., and London, 1963.
(13) J. B. Goodenough, *Bull. Soc. Chim. France*, **4**, 1200 (1965).
(14) H. Schäfer, G. Schneidereit, and W. Gerhardt, *Z. Anorg. Allgem. Chem.*, **319**, 327 (1963).
(15) F. A. Cotton and J. T. Mague, *Inorg. Chem.*, **5**, 317 (1966).
(16) J. M. Fletcher, W. E. Gardner, B. F. Greenfield, M. J. Holdoway, and M. H. Rand, *J. Chem. Soc., A*, 653 (1968).
(17) H. Schäfer, "Chemical Transport Reactions," Academic Press, New York, and London, 1964.

in an evacuated, sealed silica tube. The volume of the tube was about 10 cm³ after sealing, and the excess $NaClO_3$ was sufficient to provide about 1 atm of oxygen at growth temperature after complete oxidation of Os to OsO_2. Decomposition of $NaClO_3$ and simultaneous Os oxidation were accomplished by slowly heating the tube and its contents to 300° over 16 hr and subsequently firing at 650° for an additional 3 hr. This treatment resulted in apparently complete decomposition of the chlorate and formation of golden OsO_2 powder in one end of the tube. The tube was then transferred to a horizontal furnace and positioned so as to provide a temperature gradient along the length of the tube. The charge of OsO_2 in one end was maintained at 960 ° (T_2), and the opposite end of the tube was held at 900 ° (T_1) for about 20 hr. The transported crystals were about 1–2 mm across a polyhedral face.

Crystals of WO_2 and β-ReO_2 were prepared by a vapor-transport process using iodine as the transporting agent. The dioxides were previously prepared by reaction of their respective metal powders and trioxides in equivalent quantities in sealed silica tubes. The tungsten reagents and rhenium metal were at least 99.99% pure; however, the purity of ReO_3 was in the range 97–99%. About 0.5 g of each dioxide in powder form was placed in a silica tube together with about 2 mg of iodine, and the tube was evacuated and sealed to provide an ampoule about 3 in. in length with a volume of about 10 cm³. Transport was then accomplished by the procedure described above for OsO_2 with T_2 = 1000 and 850° and $T_1 \approx$ 960 and 825° for WO_2 and ReO_2, respectively. WO_2 crystals were obtained only in small yield. They were golden, equidimensional, and about 0.5–1 mm across a face. ReO_2 crystals were black, possessed a columnar habit, were about 2 mm in length, and were usually twinned.

Single crystals of MoO_2 and MnO_2 were grown hydrothermally from powders of MoO_3 and MnO_2 in solutions 6 N in HCl. MoO_3 was reagent grade; MnO_2 was presynthesized from high-purity Mn metal. The reactions were carried out in sealed, thin-walled, gold tubes at 700° with an external pressure of 3000 atm. In the case of MnO_2, $KClO_3$ was added to the reactants to maintain an oxidizing atmosphere. Good crystallization occurred in both cases within 24 hr. The MoO_2 crystals were bronze-colored, equidimensional in habit, and about 1 mm across a polyhedral face. MnO_2 crystals were black, possessed a needle-like habit, and were about 1 mm in length.

As recently described elsewhere,[7] RhO_2 and PtO_2 can be synthesized at elevated pressures, either hydrothermally or anhydrously, in the presence of oxygen derived from decomposition of sodium or potassium chlorate. Under these conditions the dioxides are usually recovered as finely divided black powders and RhO_2 is contaminated with small amounts of Rh_2O_3 as a separate phase. In the earlier study[7] small yields of intergrown crystal fragments of orthorhombic PtO_2 were reported to result from anhydrous conversion of reagent grade, hexagonal PtO_2 at 700° and 3000 atm. Although powder X-ray diffraction patterns obtained on the bulk product indicated a single phase of orthorhombic PtO_2, we have subsequently found, using single-crystal precession photographs, that selected crystals have cubic symmetry and probably correspond to $Na_xPt_3O_4$. Several variations in reaction conditions have been carried out in attempts to obtain single crystals of both the rhodium and platinum dioxides; however, none of these has led to crystals sufficiently large for electrical resistivity measurements. Consequently, powders of the two dioxides were used for this purpose. The powder of PtO_2 on which measurements were performed was prepared at 65 kbars and 1100°. This product appeared to be a single phase of orthorhombic PtO_2 and chemical analysis confirmed the stoichiometry within the limits of error of the analysis as described below.

As mentioned above, RhO_2 was not obtained as a pure phase and WO_2 was obtained in yields too low to permit chemical analysis. For the other dioxides, oxygen analyses were obtained using a Leco "Nitrox 6" oxygen analyzer, which incorporates inert-gas fusion and a gas chromatographic readout. Using this technique, oxygen contents of several oxide standards have been reproducibly determined to within ±0.2% of their theoretical values. The results of the analyses are shown in Table I. In the table limits of error assigned to the oxygen to metal ratios are based on the inherent ±0.2% accuracy of the technique.

TABLE I

Oxide	Wt % oxygen — Theoret.	Found	O:M
IrO_2	14.27	14.40	2.02 ± 0.03
ReO_2	14.67	14.73	2.01 ± 0.03
OsO_2	14.40	14.49	2.01 ± 0.03
MnO_2	36.81	36.84	2.00 ± 0.02
MoO_2	25.01	25.09	2.01 ± 0.02
PtO_2	14.10	13.90	1.97 ± 0.03
RuO_2	24.05	24.24	2.02 ± 0.02

Cell dimensions of the dioxides were refined by least squares using powder data obtained with a Guinier–de Wolf camera employing monochromatized Cu $K\alpha_1$ radiation and an internal KCl standard. The films were read using a Mann film reader; d values were calculated using λ(Cu $K\alpha_1$) 1.54051 Å and a_0(KCl) = 6.2931 Å.

Electrical resistivity measurements were made on crystals by the ordinary four-probe method. The probes were indium or indium alloy ultrasonically soldered on with the aid of a micromanipulator. Irregular crystals were cut into bars so that a geometrical factor for resistivity calculation could be determined. In general, measurements were made over the temperature range 4.2–300°K.

Resistivity measurements on RhO_2 and PtO_2 powders were made under an applied pressure of 35 tons/in.² using opposed, gold-plated steel pistons as electrical contacts. These measurements were carried out over the temperature range 78–356°K.

Results

Crystallographic Parameters.—X-Ray patterns obtained on powdered samples of the crystals grown in this study were all successfully indexed on the basis of reported structures for these materials. This indexing was consistent with tetragonal symmetry for MnO_2, RuO_2, RhO_2, OsO_2, and IrO_2, monoclinic symmetry for MoO_2 and WO_2, and orthorhombic symmetry for ReO_2 and PtO_2. The ReO_2 crystals were of the high-temperature variety, as expected since they were synthesized at 825°. For many of these dioxides accurate cell dimensions have not previously been reported. The results of our least-squares refinement of data obtained on these materials are shown in Table II together with other pertinent crystallographic parameters. Comparative data from the literature for these materials and for other dioxides with rutile-related structures are also listed. The data given in the table for TcO_2 are based on our indexing of the powder pattern given by Muller, White, and Roy[18] on the basis of an MoO_2-type cell. Calculated and observed d values are given in Table III. Previously, a different monoclinic cell was reported for TcO_2 by Zachariasen;[19] however, it has been observed by Muller, *et al.*, that this cell does not

(18) O. Muller, W. B. White, and R. Roy, *J. Inorg. Nucl. Chem.*, **26**, 2075 (1962).

(19) W. H. Zachariasen, A.C.A. Program and Abstracts of Winter Meeting, F-4 (1951).

TABLE II

CRYSTAL DATA FOR MO_2 COMPOUNDS HAVING RUTILE-RELATED STRUCTURES

Compound	a	b	c	β	V	c/a	Electron Config.	Average Me-O Distance	Closest Me-Me Distance	α	Reference
SiO_2	4.176	--	2.666	--	46.49	.638	$2p^6$	1.768	2.67	.82	a
GeO_2	4.396	--	2.863	--	55.32	.651	$3d^{10}$	1.90*	2.86	.89	b
MnO_2	4.3980 ± 2	--	2.8738 ± 2	--	55.58	.653	$3d^3$	1.90*	2.87	--	c
CrO_2	4.4219 ± 5	--	2.9162 ± 3	--	57.02	.660	$3d^2$	1.905	2.92	.91	d
	4.4190 ± 5	--	2.9176 ± 3	--	56.97	.661	"		"		e
VO_2 (tetr)	4.552 ± 1	--	2.846 ± 1	--	58.97	.625	$3d^1$		2.85		f
VO_2 (mon)	5.743	4.517	5.375	122.61	58.73	--	"				g
	5.7515 ± 7	4.5252 ± 5	5.3819 ± 8	122.60	59.00	-- ‡	"				c
	5.7517	4.5278	5.3825	122.65	59.00	(.626) ‡	"	1.937	2.62	.97	h
RhO_2	4.4862 ± 3	--	3.0884 ± 2	--	62.15	.688	$4d^5$	1.98*	3.09	--	i
TiO_2	4.594	--	2.958	--	62.43	.644	$3d^0$	1.959	2.96	.89	j,r
RuO_2	4.4906 ± 2	--	3.1064 ± 2	--	62.64	.692	$4d^4$	1.971	3.11	.89	c,s
IrO_2	4.4990 ± 2	--	3.1546 ± 2	--	63.85	.701	$5d^5$	1.99*	3.15	--	c
	4.4983	--	3.1544	--	63.84	.701	"		"		k
PtO_2	4.4867 ± 4	4.5366 ± 4	3.1375 ± 5	--	63.85	(.694)	$5d^6$	1.99*		--	i
α-ReO_2	5.562	4.838	5.561	120.87	64.25	(.576)	$5d^3$	1.99*	(2.49) ‡‡	--	l
OsO_2	4.4968 ± 2	--	3.1820 ± 2	--	64.36	.708	$5d^4$	1.99*	3.18	--	c
TcO_2	5.55 ± 1	4.85 ± 1	5.62 ± 1	121.9 ± 1	64.2	(.586)	$4d^3$	2.00*		--	c,t
MoO_2	5.584	4.842	5.608	120.94	65.05	--	$4d^2$				i
	5.6109 ± 8	4.8562 ± 6	5.6285 ± 7	120.95	65.76	(.577)	"	2.011	2.51	1.11	m
	5.607 ± 1	4.860 ± 1	5.624 ± 1	120.94	65.73	--	"				c
WO_2	5.656	4.892	5.650	120.69	66.139	--	$5d^2$	2.01*	(2.49) ‡‡	--	l
	5.5607 ± 5	4.9006 ± 5	5.6631 ± 5	120.44	66.53	(.567)	"				c
TaO_2	4.709		3.065		67.97	.651	$5d^1$	2.02*	3.06	--	n
NbO_2	13.70		5.987		70.297	(.618)	$4d^1$	2.048	2.80	1.03	o
	13.690 ± 1		5.9871 ± 3		70.13	(.618)	"				c
SnO_2	4.738		3.188		71.57	.673	$4d^{10}$	2.053	3.19	.87	p,r
PbO_2	4.955 ± 1		3.383 ± 2		83.06	.683	$5d^{10}$	2.135*	3.38	--	q

a. S. M. Stishov and N. V. Belov, Doklady Acad. Nauk SSSR 143, 951 (1962); stishovite.
b. H. E. Swanson and E. Tatge, NBS Circular, 539 Vol. VIII, 28.
c. this work; all cell dimensions determined at 25°C.
d. W. H. Cloud, D. S. Schreiber and K. R. Babcock, J. Appl. Phys. 33, 1193 (1962).
e. B. L. Chamberland, unpublished data; CrO_2 synthesized at 65 kb and 1200°C.
f. K. V. Krishna Rao, S. V. Naidu, and L. Ivengar, J. Phys. Soc., Japan, 23, 1380 (1967); cell dimensions extrapolated to 25°C.
g. G. Andersson, Acta Chem. Scand. 10, 1623 (1956).
h. J. Longo and P. Kierkegaard, personal communication.
i. R. D. Shannon, Solid State Commun., 6, 139 (1968).
j. H. E. Swanson and E. Tatge, NBS Circular 539, Vol. I, 44 (1953).
k. C. L. McDaniel and S. J. Schneider, J. Res. Natl. Bur. Stds. 71A, 119 (1967).
l. A. Magnéli, G. Andersson, B. Blomberg, and L. Kihlborg, Anal. Chem. 24, 1998 (1952).
m. B. G. Brandt and A. C. Skapski, Acta Chem. Scand. 21, 661 (1967).
n. N. Schönberg, Acta Chem. Scand. 8, 240 (1954).
o. B. Marinder, Arkiv Kemi 19, 435 (1962).
p. H. E. Swanson and E. Tatge, NBS Circular 539, Vol. I, 54 (1953).
q. T. Katz, Ann. Chim. (Phys.) 5, 5 (1950).
r. W. H. Baur, Acta Cryst. 9, 515 (1956).
s. F. A. Cotton and J. T. Mague, Inorg. Chem. 5, 317 (1966).
t. O. Muller, W. B. White, and R. Roy, J. Inorg. Nucl. Chem. 26, 2075 (1964).

α = the ratio of the oxygen-oxygen bridging distance to the average of the oxygen-oxygen distances of the remainder of the octahedral edges.
‡ - c/a values for monoclinic cells are explained in text.
‡‡ - these distances are not accurately known.
* - estimated distances determined by taking the sum of the effective ionic radii (Ref. 24).

account for the observed powder pattern. It is possible that there is more than one form of TcO_2 (as for ReO_2).

Electrical Resistivity.—In Figure 2 are plotted the temperature dependences of resistivity for MoO_2, RuO_2, WO_2, ReO_2, OsO_2, and IrO_2. The data were obtained on single crystals and, generally, in undetermined crystallographic directions. Since ReO_2 crystals were usually twinned, electrical resistivity was measured in the direction of the *a* axis, parallel to the twin plane. It can be seen from the figure that all of these materials exhibit high electrical conductivities with temperature dependences that are typical of metal-like conductors. This result is consistent with the findings of Perloff and Wold[20] for single crystals of MoO_2, of Gibart[21] for

(20) D. S. Perloff and A. Wold, "Crystal Growth, Proceedings of an International Conference on Crystal Growth," H. S. Peiser, Ed., Pergamon Press Ltd., London, 1967.
(21) P. Gibart, *Compt. Rend.*, **261**, 1525 (1965).

TABLE III

X-RAY DIFFRACTION DATA FOR TcO_2[a]

hkl	d_{calcd}	d_{obsd}	I/I_0
110	3.353	3.355	100
−202	2.449	2.448	40
−112	2.424	2.428	14
002	2.386	2.386	8
111	2.356	2.357	8
−212	2.179	2.179	2
021	2.161	2.164	2
−203	1.847	1.865	1
121	1.807	1.805	1
−213	1.726	1.732	<1
−113	1.711	1.708	12
022	1.700	1.703	21
−220	1.689	1.689	11
112	1.673	1.675	18
−313	1.543	1.544	2
013	1.511	1.506	4
−310	1.495	1.492	4
221	1.431	1.424	2
131	1.388	1.388	5
−402	1.387	1.380	2
202	1.356	1.369	2
103	1.312	1.313	3
−314	1.306	1.307	3
−404	1.221	1.222	<1
004	1.193	1.193	3
−414	1.184	1.188	2
−142	1.113	1.117	2

[a] The columns d_{obsd} and I/I_0 were taken directly from ref 18. The other columns are based on the TcO_2 cell given in Table II.

powder samples of ReO_2, and of Schäfer, Schneidereit, and Gerhardt[14] for RuO_2.

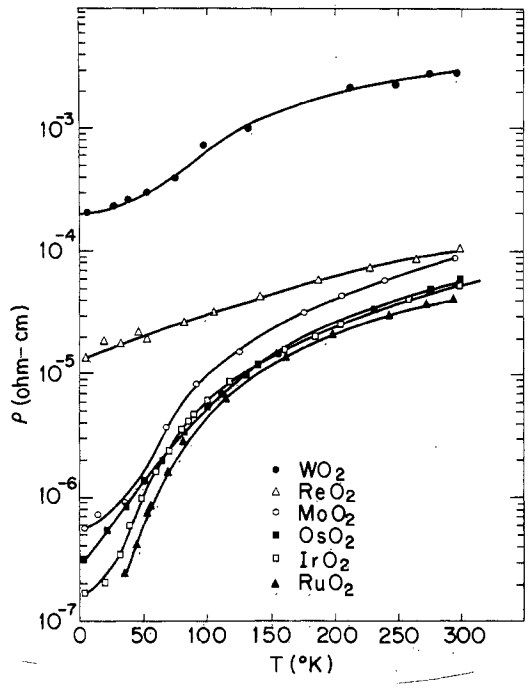

Figure 2.—Temperature dependences of electrical resistivity for the dioxides WO_2, ReO_2, MoO_2, OsO_2, IrO_2, and RuO_2.

A similar plot for a typical MnO_2 crystal is shown in Figure 3. In view of the unusual electrical behavior shown in the figure for this oxide, the measurements were repeated on numerous other crystals prepared by variations of the technique previously described. In all cases the general shapes of the ρ *vs.* T curves were similar, and all crystals exhibited the sharp drop in resistivity commencing at about 95°K.

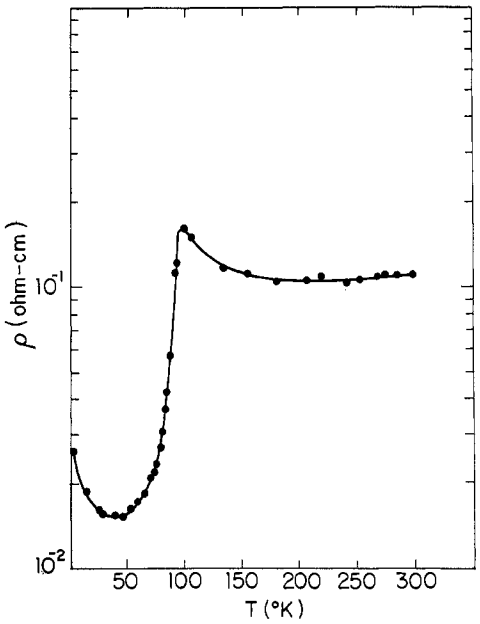

Figure 3.—Temperature dependence of the electrical resistivity of MnO_2.

The Néel temperature of MnO_2 has been reported to be 84°K.[22] However, Kelley and Moore[23] have observed a sharp exotherm in the specific heat of a carefully prepared sample of MnO_2 at 92°K and no further anomaly near the reported Néel point. Magnetic susceptibility measurements on our crystals indicated a Néel temperature at about 94°K, consistent with the specific heat effect. In view of the difficulties in obtaining stoichiometric MnO_2, we resynthesized a powder sample of this oxide in order to attempt resolution of the discrepancy in Néel temperatures. This sample was prepared by dissolving Mn metal of high purity in dilute nitric acid, carefully evaporating the resulting solution, and finally decomposing the nitrate to MnO_2 by slowly heating to 500° in air. Oxygen content of the product was 36.74 ± 0.20% to be compared with a theoretical value of 36.84%. The Néel temperature of this sample was 94°K, in agreement with the value found for the hydrothermally synthesized crystals. It would thus appear that the anomalies in electrical resistivity and specific heat at 92–95°K are associated with magnetic ordering.

We have not included in the figures electrical data for RhO_2 and PtO_2 since these data were obtained on compressed powder samples for which electrical resis-

(22) H. Bizette, *J. Phys. Radium*, **12**, 161 (1951).
(23) K. K. Kelley and G. E. Moore, *J. Am. Chem. Soc.*, **65**, 782 (1943).

TABLE IV

ELECTRICAL BEHAVIOR OF SINGLE CRYSTALS OF RUTILE-RELATED DIOXIDES

Compd	ρ(300°K), ohm-cm	ρ(4.2°K), ohm-cm	Remarks	Ref
TiO_2	$\sim 10^8$	...	$E_a \approx 1.53$ eV	*a*
VO_2	~ 10	...	Semiconducting → metallic transition at 340°K; ρ(400°K) $\approx 8 \times 10^{-4}$ ohm-cm	*b*, *c*
CrO_2	1.2×10^{-4}	2.2×10^{-6}	Ferromagnetic ($T_c = 398$°K)	*d*
MnO_2	1.1×10^{-1}	2.6×10^{-2}	Anomalous temperature dependence; transition near Néel point (94°K)	*g*
NbO_2	14	...	Semiconductor; $E_a \approx 0.26$ eV	*g*
MoO_2	2×10^{-4}	3.5×10^{-5}		*e*
	8.8×10^{-5}	5.4×10^{-7}		*g*
RuO_2	5×10^{-5}		"Metallic"	*f*
	4×10^{-5}	2.2×10^{-7}	35°K	*g*
RhO_2	$<10^{-4}$	...	Measurements made on powder sample under a pressure of 35 tons/in.^{2}; temperature dependence metal-like.	*g*
WO_2	2.9×10^{-3}	2.0×10^{-4}		*g*
β-ReO_2	1.0×10^{-4}	1.2×10^{-5}		*g*
OsO_2	6×10^{-5}	3.2×10^{-7}		*g*
IrO_2	6×10^{-5}	1.7×10^{-7}		*g*
PtO_2	$\sim 10^6$	...	Measurements made on powder under pressure of 35 tons/in.^{2} indicate semiconductivity ($E_a \approx 0.20$ eV).	*g*

[a] D. C. Cronemeyer, *Phys. Rev.*, **87**, 876 (1952). [b] F. J. Morin, *Phys. Rev. Letters*, **3**, 34 (1959). [c] P. F. Bongers, *Solid State Commun.*, **3**, 275 (1965). [d] B. L. Chamberland, *Mater. Res. Bull.*, **2**, 827 (1967). [e] D. S. Perloff and A. Wold, "Crystal Growth," Proceedings of an International Conference on Crystal Growth, H. S. Peiser, Ed., Pergamon Press Ltd., London, 1967. [f] H. Schäfer, G. Schneidereit, and W. Gerhardt, *Z. Anorg. Allgem. Chem.*, **319**, 327 (1963). [g] This work.

tivity data can at best be only qualitatively indicative of the general behavior.[24] Based on those measurements, however, it would appear that RhO_2 is probably metal-like, while PtO_2 is probably a semiconductor. Room-temperature resistivities of the compressed powders were 10^{-4} ohm-cm for RhO_2 and 10^6 ohm-cm for PtO_2. Temperature dependences of the resistivities were positive for RhO_2, as expected for a metallic conductor, and negative with a semiconductor activation energy of about 0.2 eV for PtO_2.

Electrical resistivity data obtained in this study are summarized in Table IV together with available data for other rutile-related systems. Data reported for NbO_2 were obtained on a single crystal that was kindly supplied by Professor Roland Ward.

Discussion

Magnéli and coworkers[4,8-11] pointed out that the short intercation separation within metal atom doublets in the group of dioxides with MoO_2 structure and in NbO_2 indicates the presence of strong metal–metal bonding and that a close relationship exists between the axial ratios of these rutile-related compounds and the number of free valence electrons available per bond. In VO_2 the homopolar metal bonds are broken at 340°K, and the structure transforms to that of tetragonal rutile with evenly spaced V atoms. This structural change is accompanied by transitions in electrical and magnetic properties. Morin,[25] who first pointed out the semiconductor–metal transition in this material, attributed the metallic conductivity at temperatures above the transition to the formation of a partly filled, narrow 3d (t_{2g}) band formed by overlap of neighboring cation 3d wave functions. The transition to semiconducting behavior at lower temperatures was ascribed to the onset of antiferromagnetic ordering and a consequent splitting of the partially filled band into an upper band that is empty and a set of lower, occupied levels that are localized and have an antiferromagnetic spin alignment. Goodenough[12] used a similar model for the metallic behavior, but taking into account the structural distortion and anomalous changes in magnetic susceptibility at the transition temperature, he concluded that diamagnetic cation–cation bonds are formed in the semiconducting phase with consequent localization of the electrons within the doublet clusters. He further defined a critical intercationic distance, R_c, below which metallic conductivity can be expected to occur *via* direct overlap of cationic d wave functions. Subsequently, Goodenough extended his model[13] and argued that metallic conductivity in partially ionic compounds of the transition metals may arise either by direct overlap of d wave functions or by strong covalent mixing of cationic d and anionic s,p wave functions. Applications of the latter model to rutile-related structures accounted for the occurrence of both cationic doublets and metallic conductivity in MoO_2 and permitted a rationalization of the simultaneous occurrence of ferromagnetism and metallic conductivity in CrO_2.

A schematic, one-electron energy level diagram for TiO_2 (rutile) that illustrates Goodenough's model is shown in Figure 4a. (For consistency with Figures 4b

(24) D. B. Rogers, *Solid State Commun.*, **5**, 263 (1967).
(25) F. J. Morin, *Phys. Rev. Letters*, **3**, 34 (1959).

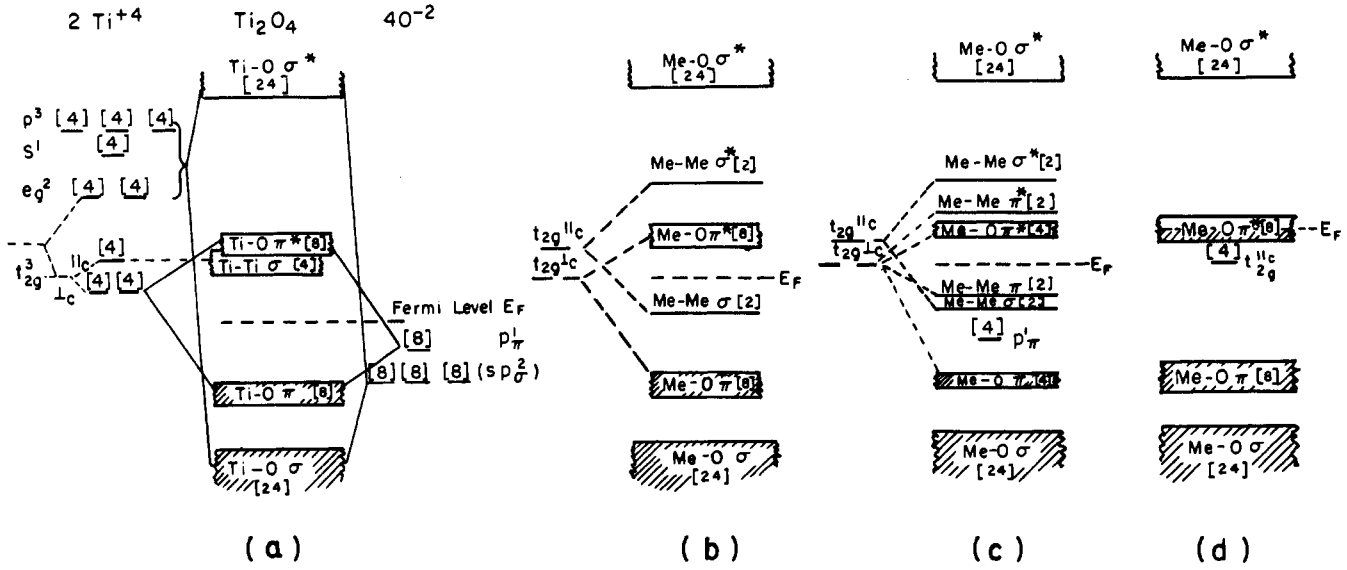

Figure 4.—Schematic, one-electron energy diagrams for rutile-related dioxides illustrating idealized models for (a) an undistorted rutile structure with strong metallic interactions parallel to the c axis, (b) a distorted structure with single M–M σ bonds, (c) a distorted structure with both M–M σ and π bonds, and (d) an undistorted structure with negligible direct M–M interactions (t_{2g} states nonbonding). All diagrams are drawn on the basis of a doubled formula, *i.e.*, M_2O_4.

and 4c, to be discussed below, the diagram is drawn for a doubled formula unit, *i.e.*, Ti_2O_4.) To construct this diagram, hybridized $e_g^2sp^3$ wave functions of the cation and sp^2 hybridized functions of the anion were assumed to interact to form bonding and antibonding σ states. Since this occurs in a polymeric crystal as opposed to a finite cluster, there are an infinite number of such states, and their *levels* are broadened into *bands* with a finite width. Bonding and antibonding bands with π symmetry can then be formed by interaction of the remaining oxygen orbital with two t_{2g} cation orbitals ($t_{2g}^{\perp}$), and, finally, a cation sublattice band can be formed by the $t_{2g}^{\parallel}$ orbitals directed along the c axis provided that the intercation separation is sufficiently small for significant overlap. The number of electrons that can be accommodated in any allowed portion of the diagram is indicated in brackets and is the product of the number of atoms per formula unit, the orbital degeneracy per atom, and the spin degeneracy per atom. In stoichiometric TiO_2, with no d electrons, the Ti–O σ and π bands are just filled, and the Fermi level lies at the middle of the energy gap between those bands and the relatively narrower antibonding π^* and cation-sublattice d bands.

Tetravalent vanadium in VO_2 possesses one d electron. In the tetragonal form of this material the overlapping π^* and cation-sublattice t_{2g} σ bands are partially filled, and the material is a metallic conductor. Below 340°K the compound transforms to the monoclinic variety in which the chains of cations sharing octahedral edges along the c axis have alternating short (2.62 Å) and long (3.17 Å) separations. This low-temperature structure implies the existence of a strong metal–metal bond between pairs of vanadium ions as suggested by Magnéli.[8,9] The effect of such bond formation on the schematic model of Figure 4a is to split the cation-sublattice $t_{2g}^{\parallel}$ σ band into a more stable, pair-localized, bonding V–V σ state below the π^* band and a less stable, antibonding state above the π^* band. This effect is illustrated in Figure 4b. Since the V–V σ level is filled with one electron per vanadium, the semiconductivity of monoclinic VO_2 is rationalized by Goodenough's model.

The model of Figure 4b also accounts rather well for the simultaneous occurrence of metal–metal doublets and metallic conductivity in MoO_2. With one more outer d electron per cation than VO_2, MoO_2 has one electron available for Mo–Mo σ bonding and an additional electron to partially fill the Mo–O π^* band. However, a difficulty arises in that the Mo–Mo separations within the pair clusters are considerably shorter than expected for the single bond predicted by the model. As mentioned previously, Marinder and Magnéli[10] showed that a high correlation exists between the metal–metal distances in certain rutile-related dioxides and the number of electrons available for bonding. This was graphically illustrated by a plot of the axial ratios of the tetragonal phases (or an analogous ratio for distorted phases) *vs.* d-electron number for zero to three d electrons per metal ion. Based on the data of Table I, we show in Figure 5 a similar, but more complete, plot for each of the transition metal dioxide series, including GeO_2, SnO_2, and PbO_2 as closed d-shell end members. The c/a ratios for the rutile pseudocells were taken to be $a/(b + c \sin \beta)$ for the monoclinic forms. In each series the plots are characterized by deep minima associated with the occurrence of cation doublets. For the first series, only VO_2 occurs at such a minimum. CrO_2 with two d electrons has a maximum axial ratio, indicating a sharp decrease in direct cation

bonding and, probably, localization of the $t_{2g}^{\parallel}$ states at discrete cation sites in this material. In the second and third transition series the minima are not realized until $n_d = 2$ and are sufficiently broad to encompass d^3 cations also. If it is assumed that the decrease in axial ratios for VO_2 and for NbO_2 is due to the formation of a single M–M σ bond, it seems likely that the continued decrease of this parameter for MoO_2 (d^2) and TcO_2 (d^3) in the second series and for WO_2 (d^2) and α-ReO_2 (d^3) in the third series is due to the formation of higher order bonds. This conclusion is further supported by Cotton's empirical correlations of metal–metal distance *vs.* bond order.[26] Comparison with his plot suggests that, whereas the M–M distances for VO_2 and NbO_2 are reasonably consistent with those expected for single bonds, the distances observed for MoO_2, WO_2, TcO_2, and α-ReO_2 are considerably closer to those expected for bond orders of two.

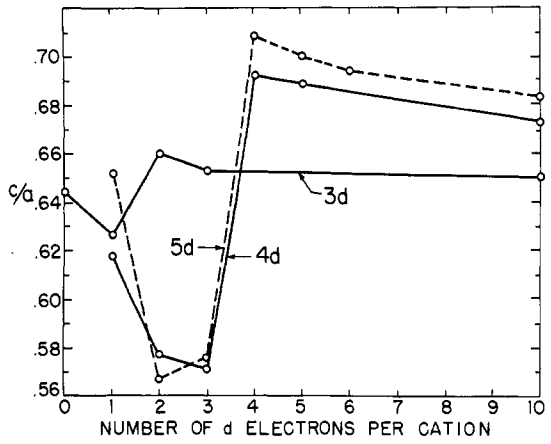

Figure 5.—Variations of the axial ratios of rutile-related dioxides with d-electron number.

Since the M–M bonding level of Figure 4b is filled with $n_d = 1$ per cation, the model does not account for the apparent occurrence of essentially double bonds with d^2 and d^3 cations. An alternate model is suggested by a recent molecular orbital calculation carried out for an $Re_2O_{10}^{31/3-}$ cluster in $La_4Re_6O_{19}$.[27] In this material the rhenium ions are octahedrally coordinated by oxygen and occur in isolated pairs in which the cations are related by octahedral edge-sharing similar to the arrangement between doublets in monoclinic variants of rutile. The short Re–Re distances in $La_4Re_6O_{19}$ are 2.42 Å as compared to approximately 2.49 Å in monoclinic ReO_2. The results of the MO calculation leave little doubt that a double bond is formed between Re ions in $La_4Re_6O_{19}$. All reasonable exponents of the Slater orbital indicated that both σ and π metal–metal bonding levels are occupied and that σ^* and π^* levels are empty. For a coordinate system with the axes nearly along the metal–ligand bonds, the Re–Re σ bond utilizes d_{xy} orbitals and the π bond utilizes one of the orbitals resulting from a linear combination of d_{xz} and d_{yz} wave functions. The other orbital resulting from this combination is available for M–O π interactions. Extension of this bonding scheme to rutile-related dioxides with metal doublets leads to the model of Figure 4c. In the figure it is assumed that the M–M π interaction has no ligand character. Actually, the calculations indicated a considerable ligand character for this bond so that Figures 4b and 4c should be considered as extreme representations of the bonding in these compounds. A hybrid of the models would permit a rationalization of both their multiple-bond and their high electrical conductivity characteristics.

The MO calculations on $La_4Re_6O_{19}$ further showed that the metal–metal bonding levels are very sensitive to the distance between the bridging oxygens as well as to the metal–metal distance. A relative measure of the variations in bridging oxygen distances can be obtained from the ratio of the distance between bridging anions to the average of the remaining interanion separations along octahedral edges. This parameter (α in Table II) is close to 0.9 for all of the rutiles where no metal–metal bonding is expected. Calculations of this ratio for the rutile fluorides (MgF_2, MnF_2, FeF_2, CoF_2, NiF_2, and ZnF_2) using the data of Baur[2,28] give very similar values. In those dioxides for which there is presumably a single bond across an octahedral edge, α is approximately unity (0.97 and 1.03 for VO_2 and NbO_2, respectively). However, in MoO_2, as well as in $La_4Re_6O_{19}$, for which double bonds are proposed, the bridging oxygens are considerably displaced from each other. In addition to shielding effects, this variation in α may be partially due to maintenance of a nearly constant cation–anion distance. When no metal–metal bonding is present, electrostatic repulsive effects dominate across the shared octahedral edges. In the rutiles this results in an elongation of the octahedra along the *c* axis. Reasonably constant cation–anion distances can be maintained under these conditions only at the expense of shorter separations between the bridging anions. Obviously, the opposite effect would result when the cations are displaced toward each other as a result of strong metal–metal bonding.

It is interesting to note that among the transition metal cations only Re^{4+} with three d electrons occurs with the unusual orthorhombic structure (β-ReO_2) characterized by zigzag chains of cations. This is perhaps rationalized by an extension of the model illustrated in Figure 4c. In the monoclinic rutile structure represented schematically by that model, only two electrons can be used in direct metal–metal interactions; the third electron would occupy an antibonding M–O π^* band in α-ReO_2. Transformation to the orthorhombic form permits bonding to two near

(26) F. A. Cotton, *Quart. Rev.* (London), **20**, 389 (1966).

(27) T. P. Sleight, C. R. Hare, and A. W. Sleight, *Mater. Res. Bull.*, **3**, 437 (1968).

(28) W. H. Baur, *Acta Cryst.*, **11**, 488 (1958); **14**, 209 (1961).

neighbors utilizing all three t_{2g} orbitals (one with σ and two with π symmetries) in metallic bonding. With three orbitals per cation bonding to two near neighbors, a bond order of about $1^1/_2$ would be expected. This prediction is in good agreement with the position of β-ReO_2 on the plot given by Marinder and Magnéli.[10] Furthermore, the equivalent of a c/a ratio in β-ReO_2 would be about 0.53, and this is substantially smaller than any other c/a ratio (Figure 5). Again, considerable ligand character is expected in these bonds, particularly for those with π symmetry.

For second- and third-row cations with d^4–d^6 and d^{10} electron configurations, as for CrO_2 and MnO_2, little direct interaction between near neighbor cations is expected on the basis of Figure 5. In general, the properties of the dioxides of these elements appear to be accounted for by the model of Figure 4d illustrated for RuO_2 (d^4) in which the $t_{2g}{}^{\parallel}$ orbital is assumed to be filled and consequently nonbonding. The metallic conductivities of the dioxides of Ru, Ir, Os, and, presumably, Rh are consistent with partial filling of the M–O π^* band. On this basis, the low, temperature-independent magnetic susceptibility of RuO_2, remarked about by Cotton and Mague[15] and by Fletcher, *et al.*,[16] would appear to be Pauli paramagnetism. For PtO_2 with six d electrons the π^* band is just filled, the Fermi level would be expected to lie in the middle of the energy gap between the π^* and σ^* bands, and semiconductivity would be expected. Although confirmation of semiconductivity for PtO_2 must await the obtaining of a single crystal of this material, our observation of high resistivity (10^6 ohm-cm) with negative temperature dependence on a powder sample provides at least qualitative consistency with the model.

Although wide variations in c/a ratios and numerous distortions from tetragonal symmetry occur in rutile-type structures, there is surprisingly little effect on the regular increase in unit cell volume with increase in the size of the cation. Thus, a plot of the cube of "effective ionic radii" ($r_c{}^3$) *vs.* the volumes of their respective rutile-like unit cells, or pseudocells, as reported earlier,[7] is remarkably linear. This linearity shows that the volume of the rutile unit cell is, to a first approximation, dependent only on ionic size and is not appreciably affected by distortions of the tetragonal cell. Contractions along the c axis caused by metal–metal bonding are compensated by an expansion along the a axis. The linearity of the plot allows the estimation of previously unknown radii of certain tetravalent, rutile-forming cations from their respective unit cell volumes reported in Table II. The radii for sixfold-coordinated Rh^{4+}, Pt^{4+}, Re^{4+}, Os^{4+}, W^{4+}, Ta^{4+}, and Pb^{4+} have been estimated to the nearest 0.005 Å and are given in Table V.

TABLE V

ESTIMATED EFFECTIVE IONIC RADII (CN VI) OF SOME TETRAVALENT IONS

Ion	Radius, Å	Ion	Radius, Å
Rh^{4+}	0.615	W^{4+}	0.65
Pt^{4+}	0.63	Ta^{4+}	0.66
Re^{4+}	0.63	Pb^{4+}	0.775
Os^{4+}	0.63		

Acknowledgments.—The authors wish to thank Miss M. S. Licis for assistance in obtaining X-ray data. Dr. J. F. Weiher carried out the magnetic measurements on MnO_2. We are also indebted to Professor Roland Ward, who loaned us a crystal of NbO_2 for electrical resistivity measurements.